PHYSICAL REVIEW E **78**, 036320 (2008)

# Alternative drag coefficient in the wake of an isolated bluff body

Md. Mahbub Alam and Y. Zhou*

*Department of Mechanical Engineering, The Hong Kong Polytechnic University Hung Hom, Kowloon, Hong Kong*

(Received 2 January 2008; revised manuscript received 20 May 2008; published 22 September 2008)

An alternative drag coefficient $C_d^a\,[=\bar{F}/(\frac{1}{2}\rho U_\infty^2 U_\infty T_s)]$, is proposed for an isolated bluff-body wake, where $\bar{F}$ is the drag force on the body per unit length, $U_\infty$ is the free-stream velocity, $\rho$ is the density of fluid, and $T_s$ is the vortex shedding period. Theoretical analysis presently conducted indicates that, while the conventional drag coefficient $C_d\,[=\bar{F}/(\frac{1}{2}\rho U_\infty^2 d)]$ may be interpreted as the intensity of the mean kinetic energy deficit distributed over the characteristic length of cylinder height $d$, $C_d^a$ is the intensity of the mean kinetic energy deficit distributed over the characteristic length of the Karman vortex wavelength $U_\infty T_s$. Therefore, $C_d^a$ may be considered to be a drag coefficient with the characteristic length given by $U_\infty T_s$, instead of $d$. As long as a bluff body is isolated, without energy exchange between the cylinder and its support, this drag coefficient is invariant, as confirmed by our experimental data as well as those in the literature, with respect to the bluff-body geometry, angle of attack, and Reynolds number, with a caveat of limited cases examined presently.

DOI: 10.1103/PhysRevE.78.036320 PACS number(s): 47.27.Ak, 47.85.Gj

## I. INTRODUCTION

A bluff-body wake is in general characterized by the Karman vortex street, irrespective of the cross-sectional geometry of bluff bodies. The flow-governing Reynolds number ($\mathrm{Re}\equiv U_\infty d/\nu$, where $d$ is the lateral dimension of the body, $U_\infty$ is the free-stream flow velocity, and $\nu$ is the kinetic viscosity of fluid) is intrinsically connected to the Strouhal number (St), the drag coefficient ($C_d$), and the parameters describing the vortex street, e.g., the vortex formation length and the wake width. In general, a shorter vortex formation length or wider wake corresponds to a lower St and higher $C_d$, and vice versa.

The definitions of St $(=f_s d/U_\infty)$ and $C_d$ $[=\bar{F}/(\frac{1}{2}\rho U_\infty^2 d)]$, where $\bar{F}$ is the drag force on a bluff body per unit length and $\rho$ is the density of fluid, have implicitly specified the cross-stream width of the bluff body as the characteristic length and the free-stream velocity as the characteristic velocity, where $f_s$ is the vortex shedding frequency. Both St and $C_d$ depend on the cross-section geometry of the body and Re. Attempt has been made to find alternative characteristic length and velocity for the sake of searching for a universal St that does not depend on the body geometry and Re. A new Strouhal number $\mathrm{St_{FG}}=\mathrm{St}d'/d=f_s d'/U_\infty$ is proposed in Ref. [1] and the St of several different cylinders collapsed to $\mathrm{St_{FG}}=0.28$, where the characteristic length $d'$ is the spacing between the shear layers. This Strouhal number is improved as $\mathrm{St}_R=\mathrm{St_{FG}}U_\infty/U_s=f_s d'/U_s$ in Ref. [2] and a value of 0.164 for the bluff bodies of different cross-sectional geometry was obtained, where $U_s$ is the flow velocity just outside the boundary layer at the separation point. The lateral separation $h$ of the two vortex rows and the convection velocity $U_c$ of vortices are suggested as the characteristic length and velocity, respectively, in Ref. [3]. In Ref. [4], the lateral distance between the maxima of streamwise fluctuating velocity measured at the end of the vortex formation length is used as the characteristic wake width.

The data in the literature point to a correlation between $C_d$ and St. Inversely related St and $C_d$ in a circular cylinder wake for Re up to $10^5$ was observed (see, e.g., Refs. [5,6]). Decreasing $C_d$ accompanied by an increasing St in the wake of a circular cylinder was noted in Ref. [7], as Re varied in the range of 50–300; a sudden increase in St was accompanied by a substantial drop in $C_d$ when Re was in the order of $10^5$, where the laminar-turbulent transition occurred in the boundary layer around the cylinder. This transition postponed flow separation and caused the wake width to shrink. For $\mathrm{Re}>3\times10^6$, $C_d$ increased again and the formation of periodical turbulent wake structures restarted. The inversely related St and $C_d$ was reconfirmed in Ref. [8]. In spite of all these experimental observations, there has not been any theoretical analysis to connect St and $C_d$ and interpret physically their relationship. Furthermore, the determination of $C_d$, which depends on many parameters such as the cross-sectional geometry of bluff bodies, the angle of attack and Re, is important both fundamentally and practically. There has been so far no attempt to find an alternative definition of drag coefficient that could allow the drag coefficients of different bluff bodies, the angle of attack and Re to collapse to a single value. The issues motivate present theoretical analysis.

The analysis is compared with experimental data obtained presently as well as previously. The bluff bodies of four different cross-sectional geometries were examined (Fig. 1). Aerodynamically, two-dimensional bluff bodies can be divided into three categories: (i) bodies with sharp edges (e.g., square and triangular cylinders), where the flow separation point is fixed; (ii) bodies with continuous surface curvature (e.g., circular and elliptical cylinders), where flow separation may occur over a segment of the surface, depending on the surface condition, Re, etc.; (iii) bodies where flow separation occurs in a restricted range of the surface such as a square prism of rounded corners and a D-shaped cylinder. The three

*Corresponding author: mmyzhou@polyu.edu.hk

 

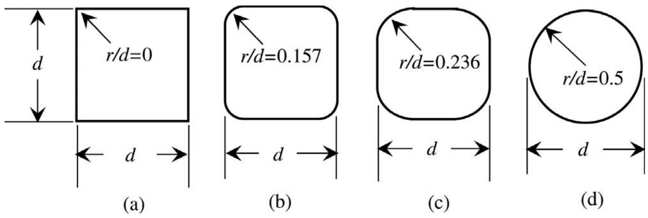


FIG. 1. Cross-sectional geometry of bluff bodies examined, where $d=12.7$ mm and $r$ is the corner radius.

types of bodies are represented by the bodies shown in Figs. 1(a) and 1(d) and Fig. 1(b) or 1(c), respectively.

## II. DRAGS AND KINETIC ENERGIES IN THE WAKE

### A. Theoretical consideration

Assume a long cylindrical bluff body with a characteristic height $d$ subjected to a uniform incompressible incoming flow at a velocity $U_\infty$. Consider a control volume, $A$-$A$-$A'$-$A'$-$A$, of unit depth in the spanwise direction (Fig. 2). Although the energy input to the control volume is steady, the energy output from it consists of two components, namely, the energies carried by the mean (time-averaged) and fluctuating mass flow through $A'$-$A'$, respectively. Denote the mean kinetic energy input to and output from the volume of unit depth in the period $T_s$ of vortex shedding from the cylinder as $K_{\text{in}}^m$ $(=K_{\text{in}}^{\text{tot}}-K_{\text{in}}^t)$ and $K_{\text{out}}^m$ $(=K_{\text{out}}^{\text{tot}}-K_{\text{out}}^t)$, respectively, where the superscripts "tot," "$m$," and "$t$" stand for "total," "mean," and "turbulent," respectively; "in" and "out" denote input to (through $A$-$A$) and output from (through $A'$-$A'$) the volume, respectively. As the input flow through $A$-$A$ is uniform and steady, $K_{\text{in}}^t=0$, that is, $K_{\text{in}}^m=K_{\text{in}}^{\text{tot}}$.

In a long cylinder case, the flow velocity in the near wake may be given by $U=\bar{U}+u$, $V=\bar{V}+v$ and $W=\bar{W}+w=w$ in the streamwise ($x$), lateral ($y$), and spanwise ($z$) directions, respectively, where overbar denotes time averaging over $T_s$ and $u$, $v$ and $w$ are the fluctuating velocities. $K_{\text{in}}^m$ can be calculated by integrating the velocity profiles across the wake, viz.,

$$K_{\text{in}}^m = \int_{-\infty}^{\infty}\int_0^{T_s} \rho U_\infty\left(\frac{1}{2}U_\infty^2\right)dtdy, \tag{1}$$

where $\rho$ is the density of fluid, $\rho U_\infty$ is the mass flow rater per unit area, and $\frac{1}{2}U_\infty^2$ is the free-stream kinetic energy per unit mass. Similarly,

$$K_{\text{out}}^{\text{tot}} = \int_{-\infty}^{\infty}\int_0^{T_s}\left\{\frac{1}{2}\rho(\bar{U}+u)[(\bar{U}+u)^2+(\bar{V}+v)^2+w^2]\right\}dtdy, \tag{2}$$

$$K_{\text{out}}^m = \int_{-\infty}^{\infty}\int_0^{T_s}\left\{\frac{1}{2}\rho\bar{U}[(\bar{U}+u)^2+(\bar{V}+v)^2+w^2]\right\}dtdy, \tag{3}$$

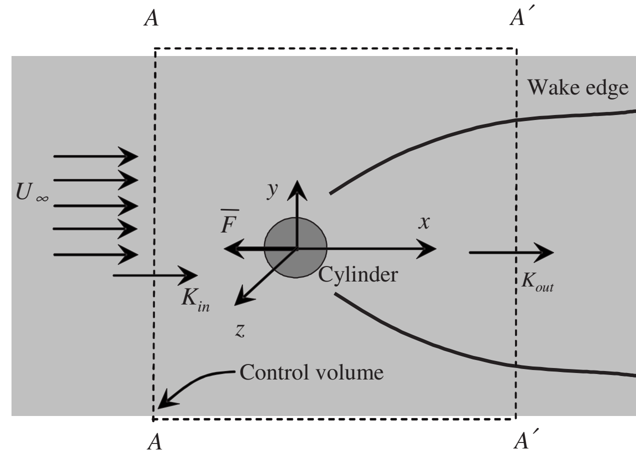


FIG. 2. Sketch of a control volume enclosing the cylinder and part of its wake. $\bar{F}$ is the time-averaged longitudinal force that the cylinder exerts on fluid. $K_{\text{in}}$ and $K_{\text{out}}$ are the total kinetic energy input and output of the control volume in one vortex shedding period, respectively.

$$K_{\text{out}}^t = \int_{-\infty}^{\infty}\int_0^{T_s}\left\{\frac{1}{2}\rho u[(\bar{U}+u)^2+(\bar{V}+v)^2+w^2]\right\}dtdy. \tag{4}$$

Based on the conservation of energy, the work done by the time-averaged drag in one vortex shedding period is given by

$$\bar{F}U_\infty T_s = K_{\text{in}}^m - K_{\text{out}}^m, \tag{5}$$

where $\bar{F}$ is the magnitude of time-averaged drag force per unit spanwise length but opposite in direction. Note that pressure energy is not considered here; its effects are negligible, as discussed later. $K_{\text{in}}^m-K_{\text{out}}^m$ may be referred to as the mean kinetic energy deficit $K_d^m$ in the wake, given by

$$\begin{aligned}K_d^m &= K_{\text{in}}^m - K_{\text{out}}^m\\ &= \int_{-\infty}^{\infty}\int_0^{T_s}\frac{1}{2}\rho U_\infty U_\infty^2 dtdy\\ &\quad - \int_{-\infty}^{\infty}\int_0^{T_s}\left\{\frac{1}{2}\rho\bar{U}[(\bar{U}+u)^2+(\bar{V}+v)^2+w^2]\right\}dtdy\\ &= \frac{1}{2}\rho U_\infty^3\int_{-\infty}^{\infty}\int_0^{T_s}[1-\bar{U}^*\{(\bar{U}^*+u^*)^2\\ &\quad +(\bar{V}^*+v^*)^2+w^{*2}\}]dtdy,\end{aligned} \tag{6}$$

where an asterisk stands for normalization by $U_\infty$.

Normalize $K_d^m$ by the input kinetic energy $(\frac{1}{2}\rho U_\infty^3 T_s d)$ carried by the free-stream fluid passing through a lateral height $d$, viz.,

$$K_d^{m^+} = \frac{K_d^m}{\frac{1}{2}\rho U_\infty^3 T_s d} = \frac{\int_{-\infty}^{+\infty}\int_0^{T_s}[1-\bar{U}^*\{(\bar{U}^*+u^*)^2+(\bar{V}^*+v^*)^2+w^{*2}\}]dtdy}{T_s d}$$

$$= \frac{1}{T_s d}\left(\int_{-\infty}^{+\infty}\int_0^{T_s}\{1-(\bar{U}^{*3}+2\bar{U}^{*2}u^*+\bar{U}^*u^{*2}+\bar{U}^*\bar{V}^{*2}+2\bar{U}^*\bar{V}^*v^*+\bar{U}^*v^{*2}+\bar{U}^*w^{*2})\}\ dtdy.\right.$$

Note that $\frac{1}{T_s}\int_0^{T_s}2\bar{U}^{*2}u^*dt=\frac{1}{T_s}\int_0^{T_s}2\bar{U}^*\bar{V}^*v^*dt=0$, $\frac{1}{T_s}\int_0^{T_s}\bar{U}^*u^{*2}dt =\bar{U}^*\overline{u^{2}}^*$, $\frac{1}{T_s}\int_0^{T_s}\bar{U}^*v^{*2}dt=\bar{U}^*\overline{v^2}^*$, and $\frac{1}{T_s}\int_0^{T_s}\bar{U}^*w^{*2}dt=\bar{U}^*\overline{w^2}^*$. Therefore,

$$K_d^{m^+} = \frac{1}{d}\int_{-\infty}^{+\infty}(1-\bar{U}^{*3}-\bar{U}^*\overline{u^2}^*-\bar{U}^*\bar{V}^{*2}-\bar{U}^*\overline{v^2}^* - \bar{U}^*\overline{w^2}^*)dy. \tag{7}$$

The integral $\int_{-\infty}^{+\infty}(1-\bar{U}^{*3}-\bar{U}^*\overline{u^2}^*-\bar{U}^*\bar{V}^{*2}-\bar{U}^*\overline{v^2}^* -\bar{U}^*\overline{w^2}^*)dy$ is the summation of the dimensionless mean kinetic energy deficit across the wake. Therefore, $K_d^{m+} =\frac{1}{d}\int_{-\infty}^{+\infty}(1-\bar{U}^{*3}-\bar{U}^*\overline{u^2}^*-\bar{U}^*\bar{V}^{*2}-\bar{U}^*\overline{v^2}^*-\bar{U}^*\overline{w^2}^*)dy$ may be interpreted as the intensity of the mean kinetic energy deficit distributed over the cylinder height.

The normalized total kinetic energy deficit $K_d^{\text{tot}+}$ and turbulent kinetic energy deficit $K_d^{t+}$ can be similarly derived, viz.,

$$K_d^{\text{tot}^+} = \frac{K_{\text{in}}^{\text{tot}}-K_{\text{out}}^{\text{tot}}}{\frac{1}{2}\rho U_\infty^3 T_s d} = \frac{\int_{-\infty}^{\infty}\int_0^{T_s}\frac{1}{2}\rho U_\infty^3 dtdy - \int_{-\infty}^{+\infty}\int_0^{T_s}\left\{\frac{1}{2}\rho(\bar{U}+u)[(\bar{U}+u)^2+(\bar{V}+v)^2+w^2]\right\}dtdy}{\frac{1}{2}\rho U_\infty^3 T_s d}$$

$$= \frac{1}{T_s d}\int_{-\infty}^{+\infty}\int_0^{T_s}\{1-(\bar{U}^{*3}+3\bar{U}^{*2}u^*+3\bar{U}^*u^{*2}+\bar{U}^*\bar{V}^{*2}+2\bar{U}^*\bar{V}^*v^*+\bar{U}^*v^{*2}+\bar{V}^{*2}u^* + u^*v^{*2}+2\bar{V}^*u^*v^*+u^{*3}+\bar{U}^*w^{*2}+u^*w^{*2})\}dtdy$$

$$= \frac{1}{d}\int_{-\infty}^{+\infty}\{1-\bar{U}^{*3}-3\bar{U}^*\overline{u^2}^*-\bar{U}^*\bar{V}^{*2}-\bar{U}^*\overline{v^2}^*-2\bar{V}^*\overline{uv}^*-\bar{U}^*\overline{w^2}^*\}dy, \tag{8}$$

$$K_d^{t^+} = \frac{0-K_{\text{out}}^t}{\frac{1}{2}\rho U_\infty^3 T_s d} = \frac{-\int_{-\infty}^{+\infty}\int_0^{T_s}\left\{\frac{1}{2}\rho u[(\bar{U}+u)^2+(\bar{V}+v)^2+w^2]\right\}dtdy}{\frac{1}{2}\rho U_\infty^3 T_s d} = -\frac{1}{d}\int_{-\infty}^{+\infty}\{2\bar{U}^*\overline{u^2}^*+2\bar{V}^*\overline{uv}^*\}dy. \tag{9}$$

In Eqs. (8) and (9) the third order terms $\overline{u^3}^*$, $\overline{uv^2}^*$, and $\overline{uw^2}^*$ are very small, compared with $\overline{u^2}^*$, $\overline{v^2}^*$, and $\overline{uv}^*$ [9,10], and therefore have been neglected. The negative sign on the right-hand side of Eq. (9) implies that the turbulent kinetic energy is generated in the control volume due to the presence of the cylinder (the integration is positive, as shown later). It is worth mentioning that $K_d^{m+}$ may also be calculated from the difference between $K_d^{\text{tot}+}$ [Eq. (8)] and $K_d^{t+}$ [Eq. (9)].

$$\text{Rewrite Eq.(5)as } \bar{F}U_\infty T_s = K_d^{m^+}\frac{1}{2}\rho U_\infty^3 T_s d. \tag{10}$$

Dividing Eq. (10) by $1/2\rho U_\infty^3 T_s d$ yields

$$\frac{\bar{F}U_\infty T_s}{\frac{1}{2}\rho U_\infty^3 T_s d} = \frac{\bar{F}}{\frac{1}{2}\rho U_\infty^2 d} = K_d^{m^+}. \tag{11}$$

Note that

$$C_d = \frac{\bar{F}}{\frac{1}{2}\rho U_\infty^2 d}. \tag{12}$$

Combining Eqs. (7), (11), and (12), one obtains

$$\begin{aligned}
C_d = K_d^{m^+} &= \frac{\int_{-\infty}^{+\infty} (1 - \bar{U}^{*3} - \bar{U}^*\overline{u^2}^* - \bar{U}^*\bar{V}^{*2} - \bar{U}^*\overline{v^2}^* - \bar{U}^*\overline{w^2}^*)dy}{d} \\
&= \frac{\text{(Aggregated mean kinetic energy deficit across the wake)}}{\text{(body height)}} \\
&= \frac{\bar{F}U_\infty}{\frac{1}{2}\rho U_\infty^3 d} = \frac{\text{(Work done by fluid on a cylinder of height } d \text{ in unit time)}}{\text{(Kinetic energy } \textit{of} \text{ free-stream fluid passing through } d \text{ in unit time)}} \\
&= \frac{\bar{F}}{\frac{1}{2}\rho U_\infty^2 d} = \frac{\text{(Time-averaged force induced on a cylinder)}}{\text{(Free-stream dynamic pressure force on } d\text{)}}.
\end{aligned} \tag{13}$$

Based on Eq. (13), three different interpretations may be offered for $C_d$. (i) $C_d$ is equal to the normalized mean kinetic energy deficit in the wake, or the intensity of aggregated mean kinetic energy deficit distributed over the lateral height $d$ [see Fig. 3(a)], which is an extension of the argument in Ref. [8] that $C_d$ is an indicator of how much energy is injected into the flow field. (ii) $C_d$ may be considered to be the ratio of work done by fluid on a cylinder of lateral width $d$ to the kinetic energy carried by free-stream fluid passing through the same lateral width, indicating how much kinetic energy of incoming fluid impinging upon the cylinder is converted into work. (iii) $C_d$ is the ratio of the force induced on a cylinder to the free-stream dynamic pressure force on the cylinder height, indicating how much the cylinder blocks incident flow, thus generating the body surface pressure.

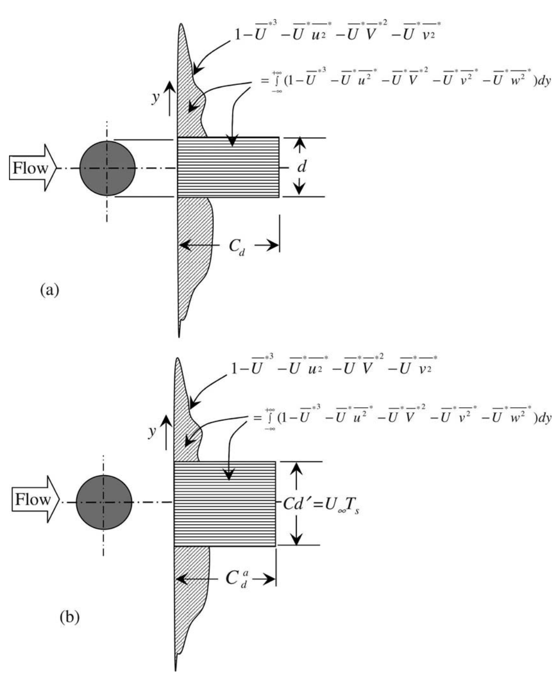


FIG. 3. Sketch of the kinetic energy deficit and interpretation of (a) $C_d$ and (b) $C_d^a$.

St is written as

$$\mathrm{St} = \frac{f_s d}{U_\infty} = \frac{d}{U_\infty T_s}. \tag{14}$$

Equation (14) suggests that St may be interpreted as the ratio of the characteristic height $d$ of a bluff body to $U_\infty T_s$, implying $U_\infty T_s$ is a characteristic length of the wake. $U_\infty T_s$ has been referred to as the vortex wavelength in the literatures (see, e.g., Refs. [8,11]) based on an assumption that vortices shed from a towing cylinder translate little with respect to ambient fluid. The convection velocity of vortices in the near wake of a circular cylinder differs, though not greatly, from the free-stream velocity [12–14], that is, $U_\infty T_s$ is not exactly the same as the vortex wavelength. $U_\infty T_s$ is likely a more appropriate characteristic length than $d$; it reflects the influences on the wake, Re, the bluff-body geometry, etc., as well as the bluff body height. In view of the fact that $C_d$ may be interpreted as the intensity of aggregated mean kinetic energy deficit distributed over the bluff body height $d$, an alternative drag coefficient $C_d^a$ may be defined as the intensity of mean kinetic energy deficit distributed over $U_\infty T_s$ [Fig. 3(b)], instead of $d$, viz.,

$$C_d^a = \frac{\int_{-\infty}^{+\infty}(1-\bar{U}^{*3}-\bar{U}^{*}\overline{u^2}^{*}-\bar{U}^{*}\bar{V}^{*2}-\bar{U}^{*}\overline{v^2}^{*}-\bar{U}^{*}\overline{w^2}^{*})dy}{U_\infty T_s}$$

$$= \frac{\frac{1}{d}\int_{-\infty}^{+\infty}(1-\bar{U}^{*3}-\bar{U}^{*}\overline{u^2}^{*}-\bar{U}^{*}\bar{V}^{*2}-\bar{U}^{*}\overline{v^2}^{*}-\bar{U}^{*}\overline{w^2}^{*})dy}{\frac{U_\infty T_s}{d}}$$

$$= K_d^{m^+}\frac{d}{U_\infty T_s} = C_d\frac{d}{U_\infty T_s} = C_d\mathrm{St}. \qquad (15)$$

Equation (15) states that $C_d^a$ is equal to the product of $C_d$ and St. Furthermore,

$$C_d^a = C_d\frac{d}{U_\infty T_s} = \frac{\bar{F}}{\frac{1}{2}\rho U_\infty^2 d}\frac{d}{U_\infty T_s} = \frac{\bar{F}}{\frac{1}{2}\rho U_\infty^2 (U_\infty T_s)}. \qquad (16)$$

Apparently, $C_d^a$ is a drag coefficient based on the characteristic length $U_\infty T_s$ instead of $d$. While $C_d$ depends on many parameters such as the Reynolds number, and bluff body geometry and orientation, it would be interesting to know whether $C_d^a$ is independent of these parameters.

### B. Experimental details

Experiments were conducted in order to verify Eq. (15) and to see whether $C_d^a$ depends on bluff body geometry. The wake was produced by four different generators, as shown in Fig. 1. $\bar{F}$ was measured using a three-component quartz piezoelectric load cell (Kistler Model 9251A). The details of the load cell were introduced in Ref. [15]. $U_\infty$ was given by a standard Pitot-static tube, placed in the free stream and connected to an electronic micromanometer (Furness Control Limited, model FCO510). $T_s$ was determined by the signal from a single tungsten wire of 5 $\mu$m in diameter, operated at an overheat ratio of 1.8 on a constant temperature circuit. The wire was placed at $x/d=2$ and $y/d=1.5$. Thus, $C_d^a$ may be estimated based on Eq. (16). A two-component laser Doppler anemometer (LDA), i.e., Dantec Model 58N40 with an enhanced FVA signal processor, was used to measure the mean velocities ($\bar{U}$, $\bar{V}$, and $\bar{W}$) and their fluctuating components ($u$, $v$, and $w$) across the wake at $x/d=2.5,4,5,6,8,10,15,20,30,40$. The coordinate system $(x,y,z)$ has already been defined in Fig. 2. The measuring volume formed by intersecting laser beams was elliptic with a minor axis of 1.18 mm and a major axis of 2.48 mm. The lateral increment between two data points was 0.5 mm or about 0.04$d$. Experiments were carried out in a closed circuit wind tunnel with a square working section (0.6 m$\times$0.6 m) of 2.4 m in length. Measurements were conducted at

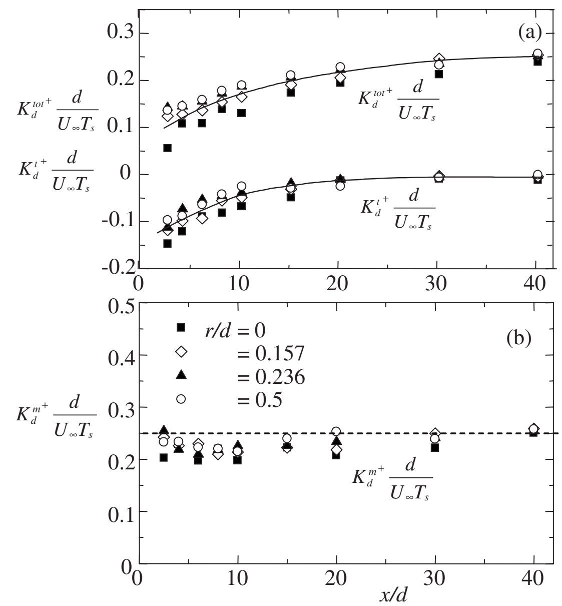


FIG. 4. (a), (b) Dependence of $K_d^{\mathrm{tot}+}\frac{d}{U_\infty T_s}$, $K_d^{t+}\frac{d}{U_\infty T_s}$, and $K_d^{m+}\frac{d}{U_\infty T_s}$ on $x/d$. The dashed line in (b) denotes measured $C_d^a(=0.25)$. Re $=2600$.

$\mathrm{Re}(\equiv U_\infty d/\nu)=2600$. The turbulence intensity of the wind tunnel is less than 0.4%. More details of the tunnel were given in Ref. [16]. $K_d^{\mathrm{tot}+}\frac{d}{U_\infty T_s}$, $K_d^{t+}\frac{d}{U_\infty T_s}$, and $K_d^{m+}\frac{d}{U_\infty T_s}$ can all be estimated from LDA measured data. The experimental uncertainties are estimated to be within 1% for $\bar{U}$, $\bar{V}$ and 3% for $\overline{u^2}$, $\overline{v^2}$, $\overline{w^2}$, and $\overline{uv}$.

## III. RESULTS AND DISCUSSION

### A. Independence of $C_d^a$ from bluff body geometry

The measured $C_d$ is 2.0, 1.7, 1.45, and 1.2 for $r/d=0$, 0.157, 0.236, and 0.5 (Fig. 1), respectively, and St is 0.128, 0.15, 0.18, and 0.21, respectively. The corresponding $C_d^a$ is 0.256, 0.255, 0.26, and 0.25, respectively. Figure 4 presents the dependence of $K_d^{\mathrm{tot}+}\frac{d}{U_\infty T_s}$, $K_d^{t+}\frac{d}{U_\infty T_s}$, and $K_d^{m+}\frac{d}{U_\infty T_s}$ on $x/d$, along with $C_d^a$. The quantities show little dependence on the cross-sectional geometry of the bluff body. The mean kinetic energy deficit $K_d^{m+}\frac{d}{U_\infty T_s}$ [Fig. 4(b)] is essentially independent of $x/d$, within experimental uncertainties, implying a negligible energy loss due to viscous dissipation, and reconfirming that the energy dissipation is very small compared to the total kinetic energy generated in the wake [8].

$K_d^{m^+}\frac{d}{U_\infty T_s}$ is further equal to $C_d^a$ ($\approx$0.25), irrespective of the body geometry, confirming Eq. (15). $K_d^{\mathrm{tot}^+}\frac{d}{U_\infty T_s}$ is smaller than $C_d^a$ at $x/d<30$, increasing from 0.12 at $x/d=2.5$ to about 0.25 at $x/d=30$. For $x/d>30$, $K_d^{\mathrm{tot}^+}\frac{d}{U_\infty T_s}$ approaches $C_d^a$, i.e., 0.25 [Fig. 4(a)]. On the other hand, $K_d^{t^+}\frac{d}{U_\infty T_s}$ is negative, implying the generation of turbulent kinetic energy in the wake, climbing from around $-0.13$ at $x/d=2.5$ to about $-0.01$ at $x/d>30$. The difference between $K_d^{\mathrm{tot}^+}\frac{d}{U_\infty T_s}$ and $K_d^{t^+}\frac{d}{U_\infty T_s}$ is independent of $x/d$ and is equal to $K_d^{m^+}\frac{d}{U_\infty T_s}$ ($=C_d^a$) for the re-

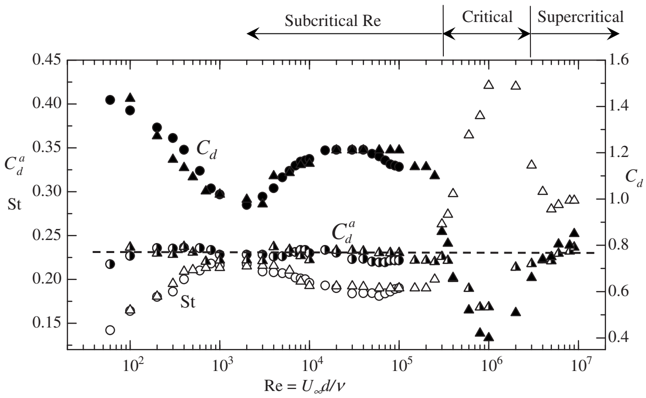


FIG. 5. Dependence of $C_d^a$ (semisolid symbols) of a circular cylinder on Re, where St (open symbols) and $C_d$ (solid symbols) were taken from Figs. 4.15 and 5.30 in Ref. [19] (circle) and from Ref. [20] (triangle). The dashed line is the best fit curve to $C_d^a$ data.

gion measured, i.e., $x/d=2.5\sim 40$ [Fig. 4(b)]. At $x/d<30$, the velocity fluctuation is vehement and the turbulent kinetic energy cannot be neglected. Therefore, $K_d^{t^+}\frac{d}{U_\infty T_s}$ accounts for the apparent difference between $K_d^{\mathrm{tot}^+}\frac{d}{U_\infty T_s}$ and $C_d^a$. As the wake develops downstream, turbulence is weakened, resulting in diminishing $K_d^{t^+}\frac{d}{U_\infty T_s}$ and increasing $K_d^{\mathrm{tot}^+}\frac{d}{U_\infty T_s}$.

Note that the pressure energy is not considered in the above discussion. However, $K_d^{m^+}\frac{d}{U_\infty T_s}$ remains approximately unchanged at different $x/d$. It seems plausible that the transform from the pressure energy to the kinetic energy or vice versa is only weakly dependent on $x/d$ and the body geometry. The mean pressure distribution along the centerline in a square-cylinder wake measured experimentally [17,18], suggested that the rate of the pressure recovery along the wake centerline be almost the same as that of the velocity recovery (see also Refs. [19–21]. For instance, at $x/d=5$, the pressure recovery was about $63\sim 69\%$ [17,18], while the velocity recovery is about 63% at Re=73.3 [20], 73% at Re=360 [21], 71% at Re=2600 [19], and 68% at Re=6000 [22].

### B. Independence of $C_d^a$ from Re

Flow behind a bluff body and hence $C_d$ and St may depend on Re. Figure 5 presents the variation of $C_d$ and St as Re increases from 60 to $10^7$ in a circular-cylinder wake. The data is extracted from the best fit curves to the experimental data in Refs. [23,24]. Although $C_d$ and St vary vigorously with Re, $C_d^a$ is approximately 0.23 in the entire Re range, except a deviation in part of the critical Re range. The deviation could be attributed to a higher uncertainty in the $C_d$ and St measurements in the critical Re range [23]. This $C_d^a$ ($\approx 0.23$) is slightly lower than the present result (Fig. 4), probably due to different experimental conditions such as cylinder aspect ratio, blockage, methods to measure $C_d$ and St.

Figure 6 presents the dependence of $C_d$, St and $C_d^a$ on Re in the case of a square cylinder, where $C_d$ and St were collected from Refs. [25–28]. Again, $C_d$ and St may vary significantly with Re; however, $C_d^a$ is approximately a constant ($\approx 0.23$) for the entire Re range.

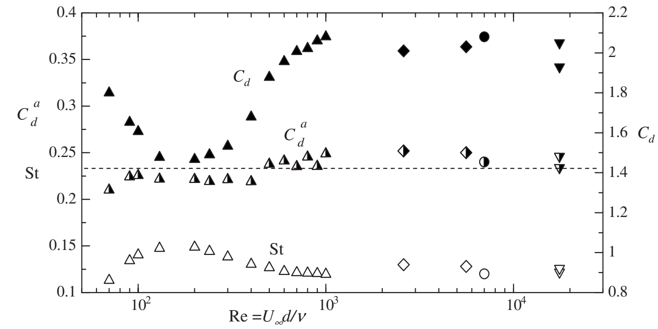


FIG. 6. Dependence of $C_d^a$ (semisolid symbols) of a square cylinder on Re, where St (open symbols) and $C_d$ (solid symbols). Triangle: Refs. [25,26]; tetragon: present; circle: Ref. [27]; reversed triangle: Ref. [28]. The dashed line is the best fit curve to $C_d^a$ data.

### C. Independence of $C_d^a$ from the orientation of a bluff body

Figure 7 presents the $C_d$ and St data measured at Re=$3\times 10^4$ in Ref. [29] in the wake of a square cylinder with the angle of attack ($\alpha$) varying from 0° to 30°. The dependence of $C_d$ and St on $\alpha$ is evident. However, $C_d^a$ is approximately a constant, 0.26, with a departure not exceeding 4%.

### D. $C_d^a$ and the base pressure parameter

It should be emphasized that Eq. (15) is derived for an isolated cylinder wake, that is, $C_d$St is invariant on condition that a cylinder is isolated, without energy exchange between the cylinder and its support. $C_d$St in a cylinder wake varied as the base pressure parameter $K$ changed from 1.3 to 1.8. $K$ is given by $(1-C_{pb})^{1/2}$, where $C_{pb}$ is the base pressure coefficient (see, Refs. [3,4]). This change in $K$ was caused by placing a splitter plate to/near the cylinder, or applying a base bleed, or forcing the cylinder to oscillate [30]. The drag on the splitter plate was not included in $C_d$ or $C_d$St in Refs. [3,4,30]; the extra energy input for base bleeding or forcing the cylinder to oscillate was not considered in Refs. [3,4]. All these contributed to a change in $C_d$St or $K_d^{m^+}\frac{d}{U_\infty T_s}$ in Eq. (15), thus causing the apparent variation in measured $C_d$St. On the other hand, $C_{pb}$ was found to vary from −0.48 at Re=50 to −1.38 at Re=$1.5\times 10^5$ in an isolated circular cylinder wake (see Fig. 8), the corresponding $K$ increasing from 1.21 to

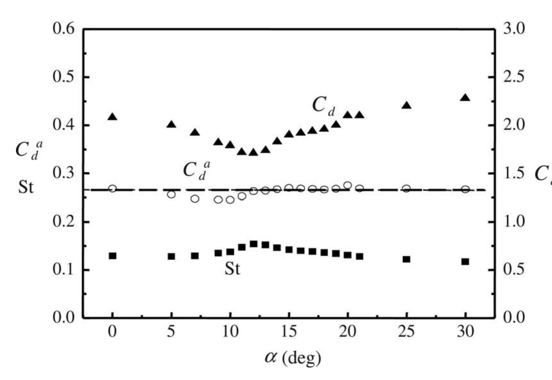


FIG. 7. Dependence of $C_d^a$ (○) on angle ($\alpha$) of attack of a square cylinder, calculated from St (■) and $C_d$ (▲) reported in Ref. [29].

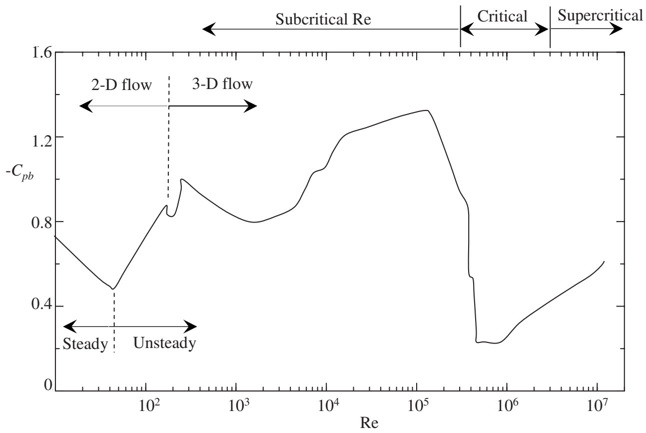


FIG. 8. Dependence on Re of base pressure coefficient of a circular cylinder, Ref. [31].

1.54. In an isolated square cylinder wake, $C_{pb}$ is $-1.65$ at $\mathrm{Re}=4.7\times10^4$ [32] and the corresponding $K$ is 1.63. However, the data in Figs. 5 and 6 indicate that $C_d^a$ is essentially unchanged over this range of Re or $K$. Unlike $C_d$, $C_d^a$ does not depend on the bluff-body geometry, orientation, and Reynolds number given an isolated cylinder without energy exchange between the cylinder and its support, which is at least valid for the limited cases examined presently.

### E. Physics behind the approximate constancy of $C_d^a$

It is of fundamental interest to understand why $C_d^a$ ($=C_d\mathrm{St}$) is approximately constant regardless of the cross section of a bluff body and Re in the subcritical regime. Following Eq. (13), $C_d$ and the kinetic energy deficit in the wake are directly related. This deficit and the wake width are further connected with each other. The wake width $d'$ is generally defined as the transverse separation between the two free shear layers in the wake (e.g., Refs. [33,34]). An alternative definition of this width is the transverse separation between the two peaks in the isocontours of the root mean square (rms) streamwise velocity in the wake [4,35,36].

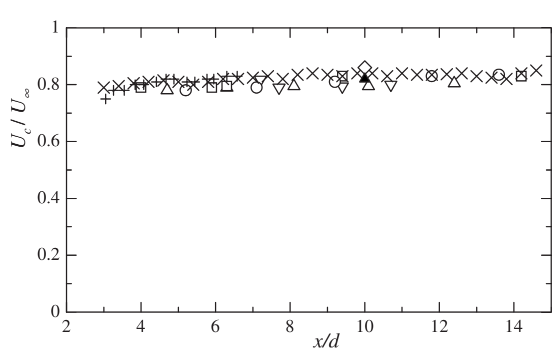


FIG. 9. Vortex convective velocity $U_c$ in a circular cylinder wake: ×, $\mathrm{Re}=10^4$, Ref. [42]; △, Re=562, Ref. [43]; □, Re=645, Ref. [43]; ∇, Re=818; Ref. [43]; ○, Re=900, Ref. [43]; +, $\mathrm{Re}=1.4\times10^5$, Ref. [44]; ◇, $\mathrm{Re}=5.6\times10^3$, Ref. [45]; ▲, Re =60–100, Ref. [46].

TABLE I. Convective velocity $U_c$ of vortices in the wake of various bluff bodies.

| Investigations | Bluff body | *Re* | $U_c/U_\infty$ |
|---|---|---|---|
| Ref. [1] | Normal flat plate, \| (angle of attack 90°) | Higher subcritical | 0.77 |
| | Circular cylinder, ● | | 0.80 |
| | Wedge, ◀ | | 0.82 |
| | Ogival, | | 0.86 |
| | Extended orgival, | | 0.81 |
| Ref. [41] | Inclined flat plate, \ (angle of attack 20°) | | 0.80 |

Karman [37] proved analytically that, given a two-dimensional invicid flow, a two-row point vortex street would be stable only if $h/a=0.28$, where $h$ is the lateral spacing between the two rows of vortices and $a$ is the longitudinal spacing between two successive vortices in each row. This condition, i.e., $h/a=0.28$, coincided with Karman and Rubach's [38] experimental data obtained in a circular cylinder wake. Benard [39] found based on his measurements that $h/a$ varied over a wide range, i.e., 0.08–0.6, for different cross-sectional geometries of bluff bodies. Hooker's [40] model demonstrated that, with the effect of vortex diffusion considered, $h$ varied and hence $h/a$ was no longer a constant. With $h$, $d'$, and $a$ measured, Fage and Johansen [1] showed again experimentally that $h/a$ was not constant and dependent on the cross-sectional geometry of a bluff body; they obtained $h/a=0.19$, 0.23, 0.29, 0.31, and 0.3 for flat plate, circular cylinder, wedge, ogival, and extended ogival, respectively. However, $d'/a$ was approximately a constant, about 0.36, for the bluff bodies examined, viz.,

$$d' = C_1 a, \tag{17a}$$

where $C_1$ is a constant, 0.36.

Apparently, $a$ may be expressed as $U_cT_s$, where $U_c$ is the convection velocity of vortices as defined in introduction. Previous studies indicate that, though increasing very slowly with $x/d$, $U_c$ is almost constant, regardless of Re and the cross-sectional geometry of a bluff body, as illustrated in Fig. 9 and Table I.

Based on the data in Fig. 9 and Table I, if we choose $U_c/U_\infty$ at $x/d=3-10$ as a reference, viz., $C_2=U_c/U_\infty\approx0.80$, then

$$a = C_2U_\infty T_s. \tag{17b}$$

Combining Eqs. (17a) and (17b) yields

$$U_\infty T_s = \frac{1}{C_1C_2}d' = Cd', \tag{17c}$$

where $C=\frac{1}{C_1C_2}\approx3.47$. Equation (17c) is fully consistent with Fage and Johansen's [1] experimental observation for different bluff bodies that $T_s$ is directly proportional to $d'$.

The fact that $U_\infty T_s$ and $d'$ are directly connected, as shown in Eq. (17c), is perhaps owing to a physical connection between $T_s$ and the bluffness of the wake generator. This bluffness directly affects the trajectory of the separating shear layer, which resembles very much to that of a projectile tossed at an angle with respect to the earth surface. For a given initial velocity, the flying time or the maximum height of the projectile grows with the increasing angle (up to 90°). Similarly, a bluffer body produces a larger lateral deflection of the separating shear layer and hence a larger $d'$ or $T_s$. It seems plausible to consider or define $d'$ or $U_\infty T_s$ as a virtual wake width or the virtual width of a bluff body. Apparently, $U_\infty T_s$ is much easier to measure than $d'$, that is, $U_\infty T_s$ is preferred to $d'$ as a characteristic length.

The approximate constancy of $C_d St$ may be deduced from the relationship between $C_d$ and $a$ for a potential flow with artificial potential point vortices in the wake. Using the stability criterion for a two-dimensional inviscid flow and potential point vortices, Karman [37] obtained

$$C_d = \frac{a}{d}\left[1.581\left(1-\frac{U_c}{U_\infty}\right) - 0.628\left(1-\frac{U_c}{U_\infty}\right)^2\right]. \quad (18a)$$

Replacing $a$ in Eq. (18a) by $U_c T_s$ yields

$$C_d = \frac{U_\infty T_s}{d}\frac{U_c}{U_\infty}\left[1.581\left(1-\frac{U_c}{U_\infty}\right) - 0.628\left(1-\frac{U_c}{U_\infty}\right)^2\right]. \quad (18b)$$

Rearranging Eq. (18b), viz.,

$$C_d\frac{d}{U_\infty T_s} = \frac{U_c}{U_\infty}\left[1.581\left(1-\frac{U_c}{U_\infty}\right) - 0.628\left(1-\frac{U_c}{U_\infty}\right)^2\right]. \quad (18c)$$

Given $\frac{U_c}{U_\infty}=0.80$, we obtain

$$C_d\frac{d}{U_\infty T_s} = 0.235, \quad (18d)$$

which is slightly lower than the present measurement, 0.25 (Sec. III A). The difference arises from the assumptions of two-dimensional potential flow and $\frac{U_c}{U_\infty}=0.80$. It may be subsequently inferred from Eqs. (18d) and (17c) that $C_d$ is approximately linearly related with $U_\infty T_s$ or $d'$.

Rewriting Eqs. (12) and (16), viz.,

$$C_d = \frac{\bar{F}}{\frac{1}{2}\rho U_\infty^2 d}, \quad (19a)$$

$$C_d^a = C_d \mathrm{St} = C_d\frac{d}{U_\infty T_s} = \frac{\bar{F}}{\frac{1}{2}\rho U_\infty^2 (U_\infty T_s)}. \quad (19b)$$

Unlike $C_d$ with $d$ used as a length scale, $C_d^a$ is normalized based on the virtual wake width (or the virtual width of a bluff body), i.e., $U_\infty T_s$. The drag coefficient under this length scale collapses for different wake generators (Figs. 4–7).

It is worth mentioning that Fage and Johansen [1] defined Strouhal number $\mathrm{St}_{\mathrm{FG}}$ based on $d'$, viz.,

$$\mathrm{St}_{\mathrm{FG}} = \frac{f_s d'}{U_\infty}. \quad (20a)$$

$\mathrm{St}_{\mathrm{FG}}$ collapsed approximately to 0.28 for different cross-sectional geometries (i.e., flat plate, cylinder, wedge, ogival, and extended ogival) of the wake generator. Noting Eq. (17c),

$$\mathrm{St}_{\mathrm{FG}} = \frac{d' f_s}{U_\infty} = \frac{d'}{U_\infty T_s} = \frac{1}{C} = 0.288, \quad (20b)$$

which is the same as Fage and Johansen's [1] observation. It may be concluded that, with the virtual wake width $U_\infty T_s$ defined as a characteristic length scale, both drag coefficient and Strouhal number collapse for different wake generators.

## IV. CONCLUSIONS

The physical relationship between an alternative drag coefficient $C_d^a$ and the mean kinetic energy deficit has been examined both analytically and experimentally. While $C_d$ may be interpreted as the intensity of the normalized mean kinetic energy deficit distributed over the length of cylinder height, $C_d^a$ is the intensity of the mean kinetic energy deficit when distributed over the length of the Karman vortex wavelength ($U_\infty T_s$), and therefore may be referred to as a drag coefficient calculated on the length scale of $U_\infty T_s$ instead of $d$. Provided that a bluff body is isolated, without energy exchange between the cylinder and its support, this drag coefficient is invariant of the bluff-body geometry, orientation, and Reynolds number, with a caveat of limited cases examined presently.

## ACKNOWLEDGMENTS

Y.Z. wishes to acknowledge support given to him by the Research Grants Council of the Government of the HKSAR through Grant No. PolyU 5334/06E. The contribution of Hu J.C. to experiments is also gratefully acknowledged.

[1] A. Fage and F. C. Johansen, Philos. Mag. **5**, 417 (1928).
[2] A. Roshko (unpublished).
[3] P. W. Bearman, J. Fluid Mech. **28**, 625 (1967).
[4] O. M. Griffin, J. Fluids Eng. **103**, 52 (1981).
[5] S. Goldstein, *Modern Developments in Fluid Mechanics* (Dover, New York, 1965).
[6] A. Roshko, Ph.D. thesis, California Institute of Technology, Pasadena, 1952.
[7] H. Oertel, Annu. Rev. Fluid Mech. **1**, 521 (1990).
[8] B. Ahlborn, L. Seto, and R. Noack, Fluid Dyn. Res. **30**, 379 (2002).
[9] Y. Zhou, R. M. C. So, M. H. Liu, and H. J. Zhang, Int. J. Heat

Fluid Flow **21**, 125 (2000).
[10] K. T. Lowe and R. L. Simpson, Int. J. Heat Fluid Flow **27**, 558 (2006).
[11] C. H. K. Williamson and A. Roshko, J. Fluids Struct. **2**, 355 (1988).
[12] B. J. Cantwell and D. Coles, J. Fluid Mech. **136**, 321 (1983).
[13] C. H. K. Williamson, J. Fluid Mech. **206**, 579 (1989).
[14] Y. Zhou and R. A. Antonia, Exp. Fluids **13**, 63 (1992).
[15] M. M. Alam and Y. Zhou, J. Fluid Mech. **589**, 261 (2007).
[16] J. F. Huang, Y. Zhou, and T. M. Zhou, Exp. Fluids **40**, 884 (2006).
[17] Y. Nakamura and Y. Ohya, J. Fluid Mech. **149**, 255 (1984).
[18] Y. Nakamura and Y. Ohya, J. Fluid Mech. **137**, 330 (1983).
[19] J. C. Hu, Y. Zhou, and C. Dalton, Exp. Fluids **40**, 106 (2005).
[20] P. Paranthoen, L. W. B. Browne, S. L. Masson, F. Dumouchel, and J. C. Lecordier, Eur. J. Mech. B/Fluids **18**, 659 (1999).
[21] J. Sung and J. Y. Yoo, J. Fluids Struct. **17**, 261 (2003).
[22] C. NorbergJ. Fluid Mech. **258**, 287 (1994).
[23] M. M. Zdravkovich, *Flow around Circular Cylinders* (Oxford University Press, Oxford, UK, 1997).
[24] A. Roshko, J. Fluid Mech. **10**, 345 (1961).
[25] A. Okajima, J. Fluid Mech. **123**, 379 (1982).
[26] A. Okajima J. Struct. Eng. **44A**, 971 (1998) (in Japanese).
[27] B. E. Lee, J. Fluid Mech. **69**, 263 (1975).
[28] S. Ootsuki, K. Fujii, H. Washizu, and S. Ohya (unpublished).
[29] T. Tamura and T. Miyagi, J. Wind. Eng. Ind. Aerodyn. **83**, 135 (1999).
[30] C. J. Apelt, G. S. West, and A. A. Szewczyk, J. Fluid Mech. **60**, 187 (1973).
[31] A. Roshko, J. Wind. Eng. Ind. Aerodyn. **49**, 79 (1993).
[32] P. W. Bearman and E. D. Obasaju, J. Fluid Mech. **119**, 297 (1982).
[33] J. H. GerrardJ. Fluid Mech. **25**, 401 (1966).
[34] S. Balachandar, R. Mittal, and F. M. Najjar, J. Fluid Mech. **351**, 167 (1997).
[35] O. M. Griffin and S. E. Ramberg, J. Fluid Mech. **66**, 729 (1974).
[36] S. E. Ramberg, J. Fluid Mech. **128**, 81 (1983).
[37] T. V. Kármán, *Collected works of Theodore van Kármán*, Vol. 1 (Butterworth, London, 1956).
[38] T. V. Kármán and H. Rubach, Phys. Z. **13**, 49 (1912).
[39] H. Benard, Compt. Rend. **182**, 1523 (1926).
[40] S. G. Hooker, Proc. R. Soc. London, Ser. A **154**, 67 (1936).
[41] K. M. Lam and M. Y. H. Leung, Eur. J. Mech. B/Fluids **24**, 33 (2005).
[42] S. Tanaka and S. Murata, Bull. JSME **29**, 1446 (1986).
[43] E. Tyler, Philos. Mag. **9**, 1113 (1930).
[44] B. J. Cantwell and D. Coles, J. Fluid Mech. **136**, 321 (1983).
[45] Y. Zhou and R. A. Antonia, Exp. Fluids **13**, 63 (1992).
[46] O. Paranthoen, L. W. B. Browne, S. L. Masson, F. Dumouchel, and J. C. Lecordier, Eur. J. Mech. B/Fluids **18**, 659 (1999).